ACS OMEGA

http://pubs.acs.org/journal/acsodf

Article

Visible-Light Driven H_2O-to-H_2O_2 Reaction by Nitrogen-Enriched Resins for Photocatalytic Oxidation of an Organic Pollutant in Wastewater

Je-Wei Hsu, Ling-Wei Wei, Wan-Ru Chen, Shou-Heng Liu, and H. Paul Wang*

Cite This: *ACS Omega* 2022, 7, 23727−23735

Read Online

ACCESS | Metrics & More | Article Recommendations

ABSTRACT: A photocatalytic H_2O-to-H_2O_2 reaction for sustainable organic wastewater treatment is environmentally attractive. Phenolic resins, inexpensive metal-free photocatalysts, are capable of harvesting visible light. Herein, novel nitrogen-enriched resin photocatalysts with a desired band-gap energy (1.83−1.98 eV) for harvesting visible light were prepared by copolymerization of resorcinol and melem for simultaneous photocatalytic H_2O-to-H_2O_2 and oxidation of methylene blue. Under visible light irradiation for 5 h, very high yields of H_2O_2 (870−975 μM of H_2O_2/g/h) by RFM resin photocatalysts could be achieved. The photocatalytic H_2O_2 for reactive oxygen species ($^{\bullet}OH$) and photogenerated h^+ could account for high conversion (40% conversion under visible light irradiation within 3 h) in oxidation of methylene blue. Such unique low-cost metal-free resins demonstrate the visible light photocatalytic H_2O-to-H_2O_2 reaction which can synergize with the oxidation of organic pollutants in wastewater.

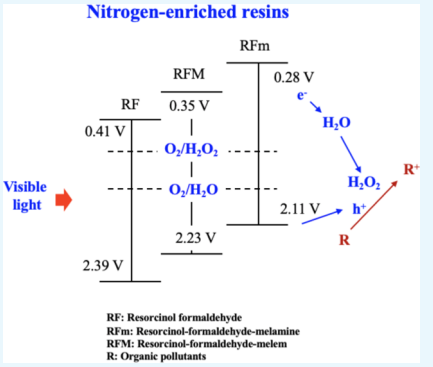

INTRODUCTION

Persistent organic pollutants (POPs) such as pharmaceuticals, pesticides, and dyes in wastewater could be degraded in an advanced oxidation process (AOP).[1] Hydrogen peroxide (H_2O_2), being an eco-friendly oxidant, could induce high reactive hydroxide radicals ($^{\bullet}OH$) for the oxidation of POPs under UV light irradiation.[2] However, H_2O_2 is generally produced by the anthraquinone method which has the main drawbacks of high energy consumption, complicated operation, potential explosion, and organic solvent pollution.[3] Therefore, the generation of H_2O_2 from H_2O via photocatalysis for the treatment of organic wastewater has received high attention mainly due to the necessity of the green process perspective for sustainable development.[4]

Photocatalysis of H_2O to H_2O_2 by semiconductors such as TiO_2, ZnO, $BiVO_4$, and WO_3 has been widely studied.[5−10] Largely due to the high recombination rate of photogenerated electrons and holes causing a low conversion efficiency, heteroatom doping, controlling morphology, co-catalyst loading, and heterojunction with other semiconductors have thus been used to improve photocatalytic efficiencies.[11−15] Although many photocatalysts have been used in photocatalytic water splitting, the following improvements are essential for commercialization: (1) Achievement of desired conversion, (2) presence of organic solvents as electron donors, (3) use of inexpensive photocatalysts, and (4) decrease of photocatalyst band-gap energy to <2 eV for visible light irradiation between 400 and 700 nm.[16] A stable and inexpensive metal-free photocatalyst was thus desirable and still challenging.

Resorcinol-formaldehyde (RF), known as a phenolic resin, could be prepared by thermal condensation for applications in drug delivery, catalyst support, super-capacitors, and absorbents.[17−20] The phenolic resins containing a band-gap energy of 1.8−2.0 eV could effectively harvest sunlight for wastewater treatment by photocatalytic oxidation of organic pollutants.[21] Also, the metal-free phenolic resin photocatalyst could be used for the generation of H_2O_2.[22] It is worth noting that the metal-free resins stably generated H_2O_2 with 0.5% of solar-chemical conversion, which is comparable to the efficiency for the photocatalytic water splitting by metal-based photocatalysts.[22,23] However, preparation of the resins involves high-temperature and high-pressure reactions. Melem, an active matter in graphitic carbon nitrides (g-C_3N_4) (GCN), is insoluble in most solvents because of the strong hydrogen bonding in tri-s-triazine that could severely hinder the grafting process with other carbon materials.[24−26] In addition, the melem unit, an active matter in GCN, could form 1,4-endoperoxide intermediates during photocatalysis which

Received: April 15, 2022
Accepted: June 14, 2022
Published: June 29, 2022

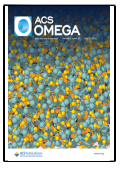

induced the formation of H_2O_2 and suppressed H_2O_2 decomposition.[27−29] In this work, novel metal-free nitrogen-enriched resins were thus prepared by a simple acidification process. The resorcinol-formaldehyde-melem resin was prepared by the copolymerization of melem and resorcinol under acidic conditions. The resorcinol crosslinked with different monomers (melem and melamine) as the visible light photocatalyst was used in photocatalytic generation of H_2O_2 and oxidation of organic pollutants in a single compartment. Different nitrogen-enriched monomers for photocatalytic generation of H_2O_2 and oxidation of a representative organic pollutant in wastewater were studied in the present work. Additionally, the photocatalytic reaction kinetics effected by the resins were also investigated for further engineering applications.

MATERIALS AND METHODS

Preparation of Resin Photocatalysts. The preparation procedures for the resorcinol-formaldehyde (RF), resorcinol-formaldehyde-melamine (RFm), and resorcinol-formaldehyde-melem (RFM) resins are briefly described in Figure 1. A

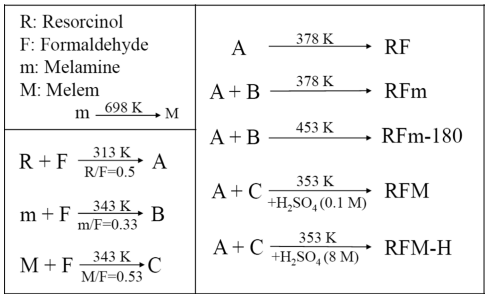

Figure 1. Preparation procedures for the resin photocatalysts.

solution of resorcinol (R) (Sigma-Aldrich, 99%) and formaldehyde (F) (Acros Organics, 37%) at the R/F molar ratio of 0.5 was mixed in deionized water (40 mL) by stirring at 353 K for 24 min. The solids were washed by acetone to eliminate impurities, filtered, and dried in an oven at 378 K to yield the RF resin.

To prepare the RFm resin, resorcinol and formaldehyde at the R/F molar ratio of 0.50 were mixed in deionized water (20 mL) under stirring at 313 K for 1 h to form solution A. Melamine (m) (Alfa Aesar, 99%) and formaldehyde at the m/F molar ratio of 0.33 were mixed in deionized water (20 mL) under stirring at 343 K until the solution become colorless to yield B. The clear solution B that was cooled down to 313 K was mixed with solution A for 30 min. The mixed solution was heated at 353 K without stirring for 24 h. The generated solids were washed by acetone to eliminate impurities, filtered, and dried at 378 K to yield brown RFm. The mixed solution containing resorcinol, formaldehyde, and melamine was also heated in a Teflon-lined autoclave at 453 K for 24 h to form the RFm-180 resin for photocatalytic studies.

Because of the strong hydrogen bond in the tri-s-triazine structure, melem (2,5,8-triamino-tri-s-triazine) (M) could not be completely dissolved in most solvents (i.e., water, DMSO, DMF, and methanol) which severely restricted the reaction in the solution with other organic compounds.[30] Nevertheless, melem has three primary amine functional groups in tri-s-triazine for protonation and dissolution with a strong acid. Melem has a high solubility (>385 mg/mL) in sulfuric acid at 298 K without chemical perturbation in the tri-s-triazine of melem, which was revealed by nuclear magnetic resonance (NMR).[24]

Melem was prepared by thermal condensation of melamine (m) at 698 K for 4 h.[31] The RFM resin was prepared by thermal condensation of resorcinol, formaldehyde, and melem with sulfuric acid to have a homogenous copolymerization. Melem and formaldehyde at the M/F molar ratio of 0.33 were mixed under magnetic stirring at 343 K for 1 h to yield solution C. The solution C was cooled down to 313 K and mixed with solution A for 30 min and heated at 353 K without stirring for 24 h. The RFM and RFM-H resins were yielded in the weak (0.1 M) and strong (8 M) acidic H_2SO_4 solutions, respectively. The suspended solids that were washed with acetone were filtered and dried at 378 K for 24 h.

Characterization of the Resin Photocatalysts. The chemical structure of the resins was studied by solid-state ^{13}C nuclear magnetic resonance (NMR) (Bruker AVANCE III HD) using a 9.4 T magnet. The UV−vis absorption spectra of the resins between 200 and 800 nm were recorded on a Varian Cary 100 diffuse reflectance spectrophotometer. $BaSO_4$ was used as a reference. The band-gap energy of the resin photocatalysts was obtained by the Tauc plot converted from their UV−vis absorption spectra. The crystalline structure of the resins was determined by X-ray diffraction (XRD) (D8 Discover, Bruker AXS Gmbh) under Cu Kα (0.1541 nm) radiation at 40 kV and 40 mA. The morphologies and particle sizes of the photocatalysts were studied by scanning electron microscopy (SEM) (UHRFE-ESM.AURIGA) and transmission electron microscopy (TEM) (JEOL JEM-2100F Cs STEM).

To understand the recombination rate of the photogenerated electrons and holes of the resin photocatalysts, their photoluminescence (PL) spectra were recorded via micro-Raman spectroscopy (Labram HR, France) using a 325 nm wavelength laser as the excitation source. The electrochemical measurements were conducted in a three electrode system using Pt and Ag/AgCl (KCl (3 M)) as the counter and reference electrodes, respectively. The photocatalysts were coated on carbon paper as the working electrodes. The resins (about 50 mg) were mixed with *N*-methyl-2-pyrrolidone (NMP) (2 mL) containing polyvinylidene difluoride (PVDF) (5 mg) as the binder, which were sonicated for 1 h to form a slurry that was evenly dripped onto a carbon paper and dried at 353 K for 2 h. The electrolyte contains the Na_2SO_4 (0.1 M) aqueous solution that was purged with nitrogen gas to remove the remaining oxygen before measurements.

Photocatalytic Studies. Photocatalytic H_2O-to-H_2O_2 reactions and oxidation of methylene blue (>89%, Sigma-Aldrich) under visible light irradiation were studied in a cylindrical glass reactor containing the photocatalysts (40 mg) and deionized water (40 mL). Prior to the photocatalytic experiments, the solution in the reactor was purged with oxygen under the dark to reach the adsorption−desorption equilibrium. A 500 W Xe lamp (Burgeon Instrument Co., Ltd.) having the light cutoff at 400 nm was used for photocatalysis at 298 K. To measure the concentration of H_2O_2, about 1 mL of the aqueous solution from the photocatalytic reactor was periodically sampled, and the solid photocatalysts were separated by filtration using a filter (0.22 μm). Concentrations of H_2O_2 at pH 5−9 could be determined with benefits of insensitivity to other byproducts in water, high stability of

https://doi.org/10.1021/acsomega.2c02371
ACS Omega 2022, 7, 23727−23735

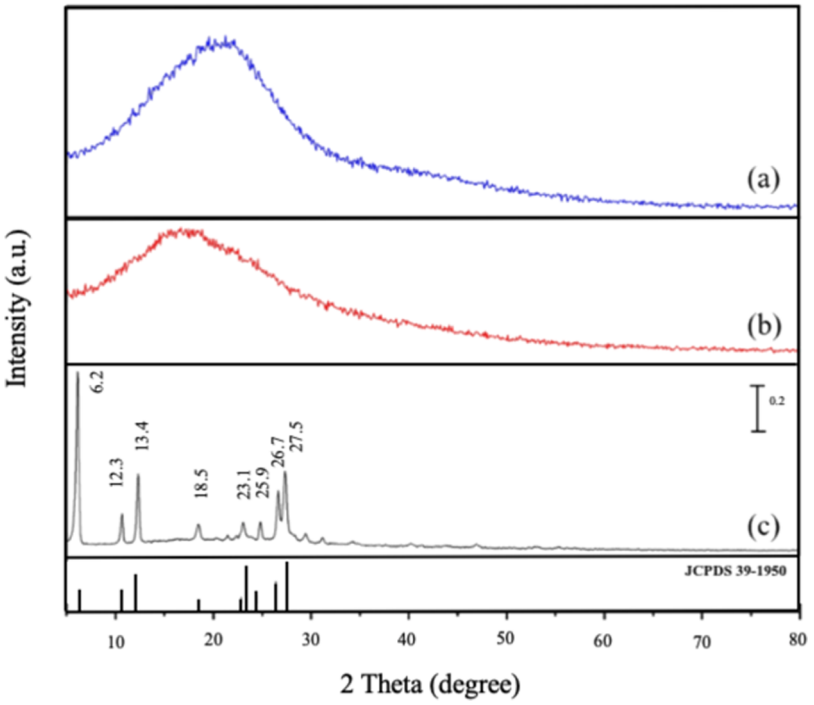

Figure 2. XRD patterns of the (a) RFm, (b) RF, and (c) RFM resins with the crystalline structure of melem (39-1950, JCPDS).

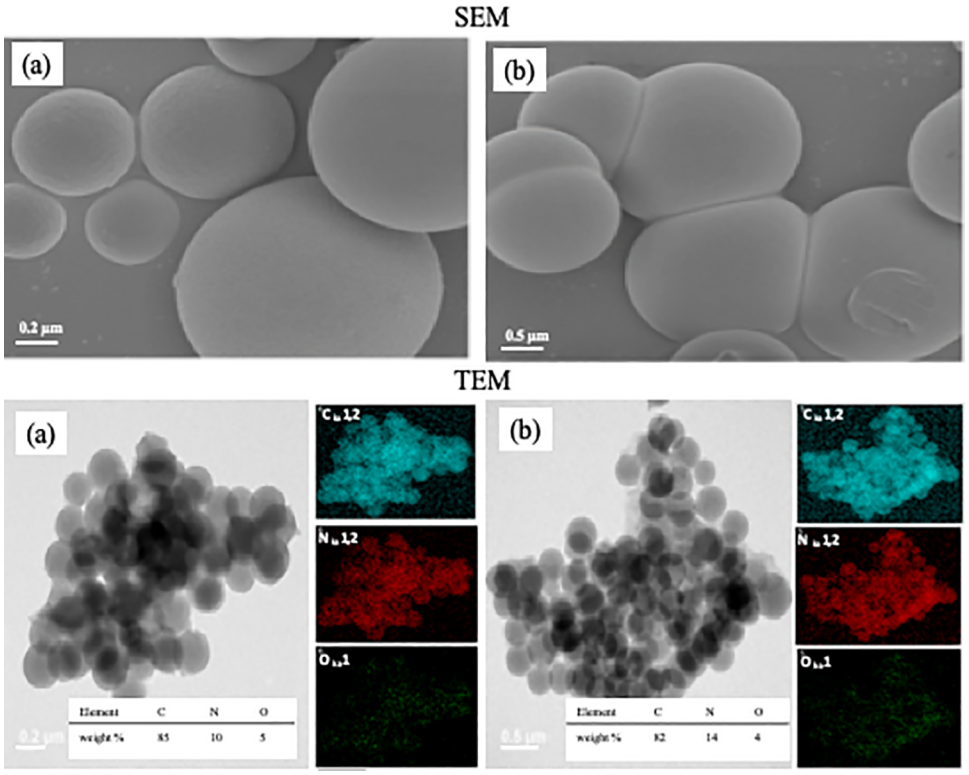

Figure 3. SEM and TEM images of the (a) RFm and (b) RFM resins. The distributions of C, N, and O in the resins are also shown in the SEM-mapping spectra.

color, and rapid reactivity. The 2,9-dimethy-1,10-phenanthroline (10 mg/mL) (DMP, 98%, Alfa Aesar) solution (0.5 mL), the copper(II) sulfate solution (0.01 M) (0.5 mL), the phosphate buffer solution (0.1 M) (0.5 mL) (pH 7), deionized water (1 mL), and the sample withdrawn from the reactor (1 mL) were mixed in a quartz tube having a 1 cm light pathway.[32] The absorbance of 454 nm was measured on an UV−vis spectrometer (Varian, Cary 100). The decomposition rate of H_2O_2 (1 mM) effected by the resin photocatalysts (40 mg) under visible light irradiation for 5 h was also measured using the copper-DMP method.

https://doi.org/10.1021/acsomega.2c02371
ACS Omega 2022, 7, 23727−23735

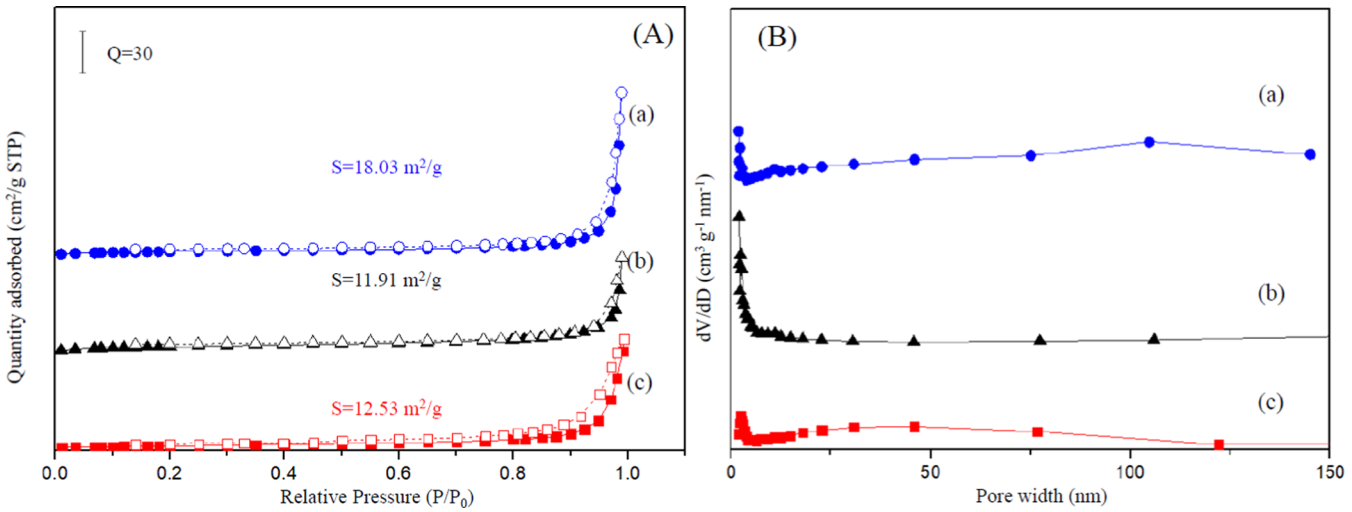

Figure 4. N_2 adsorption−desorption isotherms and pore size distributions of the (a) RFM, (b) RF, and (c) RFm resins.

Methylene blue, being a common dyestuff in industry, was used to simulate organic pollutants in wastewater. The resin photocatalysts (40 mg) were dispersed in an aqueous solution (40 mL) containing methylene blue (3×10^{-5} M) under pH 1−9 (adjusted by HCl (1 M) and NaOH (1 M)) in a cylindrical glass reactor. Before the photocatalytic oxidation of methylene blue, the solution was stirred under dark to reach the adsorption equilibrium in the reactor that was then irradiated by a 500 W Xe lamp (Burgeon Instrument Co., Ltd.) having the light cutoff at 400 nm at 298 K. The solution was sampled at a selected period and centrifuged to remove particles from water. The efficiency for the photocatalytic oxidation of methylene blue was studied by measuring the maximum absorbance at 664 nm on the UV−vis absorption spectrometer. To ensure the mineralization of methylene blue, the total organic carbon (TOC) in the reactor was determined on a total organic carbon analyzer (Shimadzu, TOC-L).

RESULTS AND DISCUSSION

Characterization of the Resin Photocatalysts. The XRD patterns in Figure 1 show that the resins have an amorphous structure at a broadened peak (5−30°) centered at 21° corresponding to the (002) plane of graphitic carbon. In addition, the RFM resin has intense peaks centered at 6.2, 12.3, 13.4, 18.5, 23.1, 25.9, 26.7, and 27.5° (2θ) that are related to the crystalline structure of melem (39-1950, JCPDS). Note that the peak at 6.2° is associated with monomer melem.[33] Morphologies of the resins (RFm and RFM) observed by TEM and SEM are shown in Figure 2. The resins appear in quasi-spheres with particle sizes in the micron scale. The sizes of the RFm and RFM resin are in the range of 20−80 μm. The well distributions of C, N, and O in the resins are also shown in the SEM-mapping spectra (Figure 3).

The N_2 absorption−desorption isotherms and pore size distributions for the RFM, RF, and RFm resins are shown in Figure 4. The resin photocatalysts exhibit type IV isotherms with H3 hysteresis loops at a high relative pressure range (P/P_0 > 0.8) (referred to as the classification of the IUPAC), suggesting the existence of mesopores. Note that the RFM has a relatively high specific surface area and pore volume.

The chemical structure of the resins was studied by ^{13}C NMR spectroscopy. Figure 5 shows that the melem units are crosslinked in the phenolic resin structure to form the RFM resin at the shifts of 164 and 154 ppm which are attributed to $C-N_2(NH_2)$ and $C-N_3$ in heptazine, respectively.[34] On the other hand, the chemical structure of the RFm resin prepared by crosslinking between melamine and resorcinol is associated with the shift at 166 ppm. The shift at 153 ppm can be attributed to C−OH, suggesting that resorcinol behaves like an electron donor in the resins.[35−37]

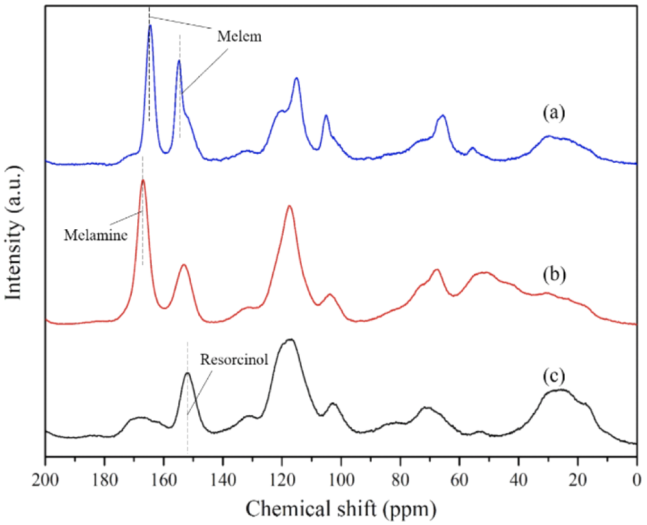

Figure 5. ^{13}C NMR shifts of the (a) RFM, (b) RFm, and (c) RF resins.

As shown in Figure 6a, the deconvoluted ^{13}C NMR of the RFM resin has 14 carbon peaks including aromatics, melem units, linkers, and unconnected functional groups between 0 and 180 ppm. The shifts in NMR attributed to the carbon in heptazine are found at 164.6 and 155.0 ppm (#1 and 2). Carbon by being substituted or without being substituted in aromatics is observed at 153.1, 131.5, 122.2, 117.8, 111.4, and 105.2 ppm (#3−8). The carbon shifts (#9, 12−14) of linkers as bridge in polymers, i.e., methylene ether, methylene and linkers between aromatic and heptazine appear at 70.7, 29.5, 19.7, and 54.5 ppm, respectively. Noncrosslinked methylol groups (C−OH) remained on the resorcinol, and melem units are related to the shifts at 60.0 and 65.9 ppm, respectively (#10, 11).

https://doi.org/10.1021/acsomega.2c02371
ACS Omega 2022, 7, 23727−23735

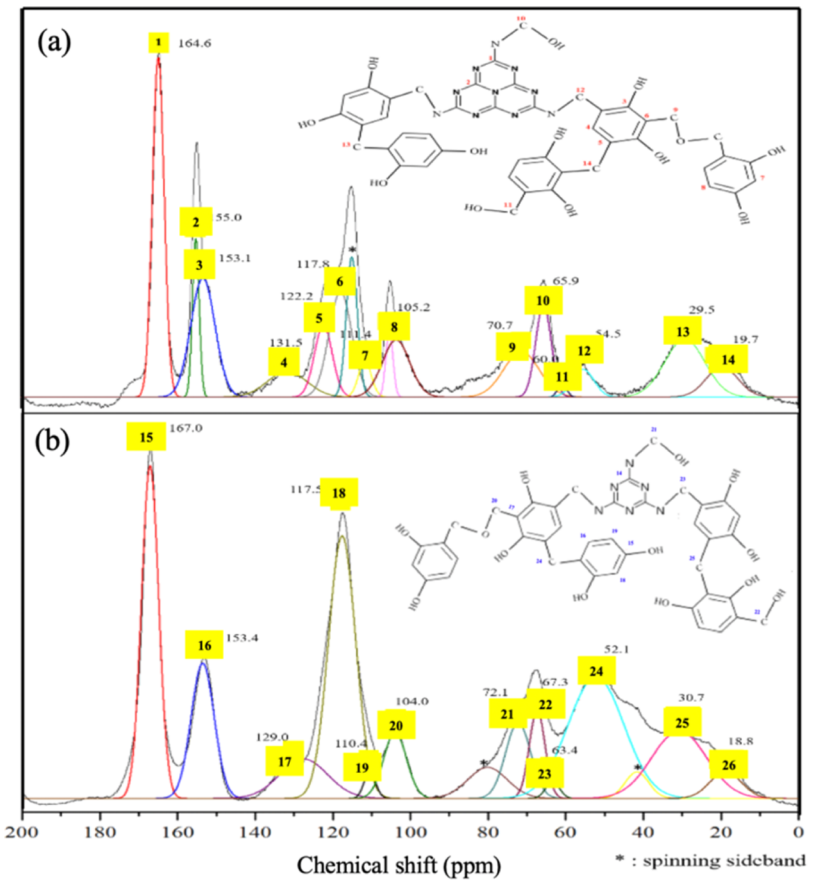

Figure 6. Deconvolution of ^{13}C NMR shifts for the (a) RFM and (b) RFm resins. Heptazine C−N_2(NR_2) [164.6 ppm, 1], Heptazine C−N_3 [155.0 ppm, 2], resorcinol C−OH [153.1 ppm, 3], nonreplaced resorcinol C [131.5ppm, 4; 111.4ppm, 7; 105.2 ppm, 8], replaced resorcinol C [122.2 ppm, 5; 117.8 ppm, 6], methylene ether linker −C−O−C− [70 ppm, 9], methylene linker [30.0 ppm,13; 20.0 ppm, 14], methylol C−OH [65.9 ppm, 10; 60.0 ppm, 11], and linker N−C−C [54.5 ppm, 12], triazine C−N_3 [167.0 ppm, 15], resorcinol C−OH [153.1 ppm, 16], nonreplaced resorcinol C [129 ppm, 17; 110.4 ppm, 19; 104.0 ppm, 20], replaced resorcinol C [117.5 ppm, 18], methylene ether linker −C−O−C− [72.1 ppm, 21], methylene linker [30.7 ppm, 25; 18.8 ppm, 26], methylol C−OH [67.3 ppm, 22; 63.4 ppm, 23], and linker N−C−C [52.1 ppm, 24].

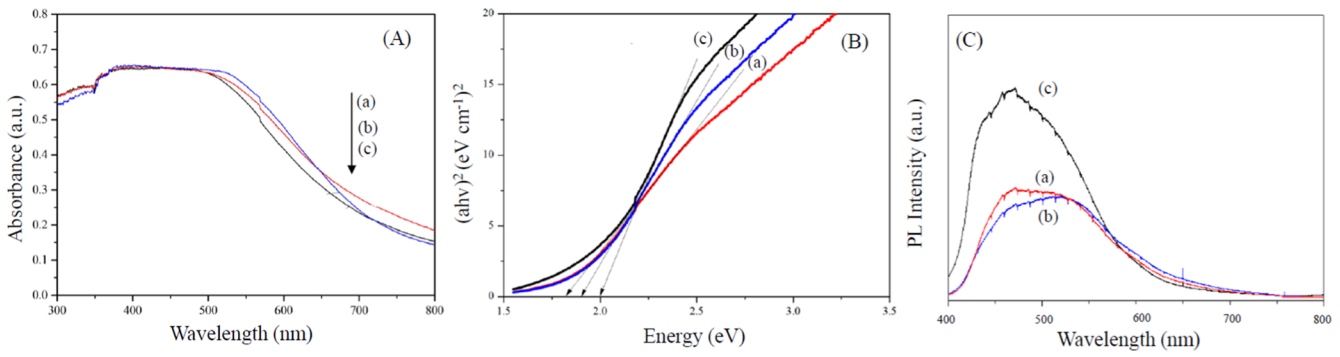

Figure 7. (A) UV−vis diffuse reflectance spectra, (B) Tauc plots, and (C) PL spectra of the (a) RFm, (b) RFM, and (c) RF resins.

Compared to the NMR shifts of the RFM resin, the melem carbon groups are substituted by the shifts of melamine at 167 ppm (see Figure 6b). The NMR shifts of aromatics, linkers, and residual functional groups (#3−14) for the RFm resin similarly correspond to those of the RFM resin (#18−26). However, the NMR shifts at similar positions of carbon components for the RFM and RFm resins are slightly different, which may be attributed to the variance in the molecular structure and electron migration property between melem and melamine.

Figure 7A shows that the UV−vis diffuse reflectance spectra of the resins have an intense absorbance between 200 and 700 nm, suggesting that the resin photocatalysts can harvest visible light. The band-gap energy of the resins was studied by the Tauc plot (see Figure 7B) obtained from the absorption spectra. The RF, RFM, and RFm resins have a band-gap energy of 1.98, 1.88, and 1.83 eV, respectively. It seems that the band-gap energy of the resins decreases by incorporating nitrogen-enriched units, such as melem and melamine. The band-gap energy could be affected by many factors such as the size of sp^2 clusters, distortion of π state, and sp^2/sp^3 contents.[38] The red-

https://doi.org/10.1021/acsomega.2c02371
ACS Omega 2022, 7, 23727−23735

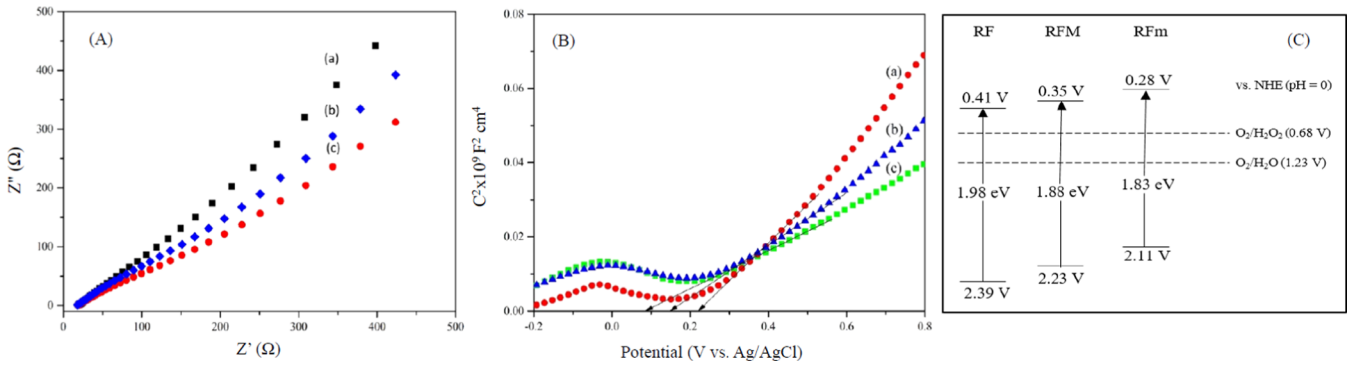

Figure 8. (A) Mott−Schottky plots, (B) EIS for the Nyquist plots, and (C) energy band levels of the (a) RF, (b) RFM, and (c) RFm resins.

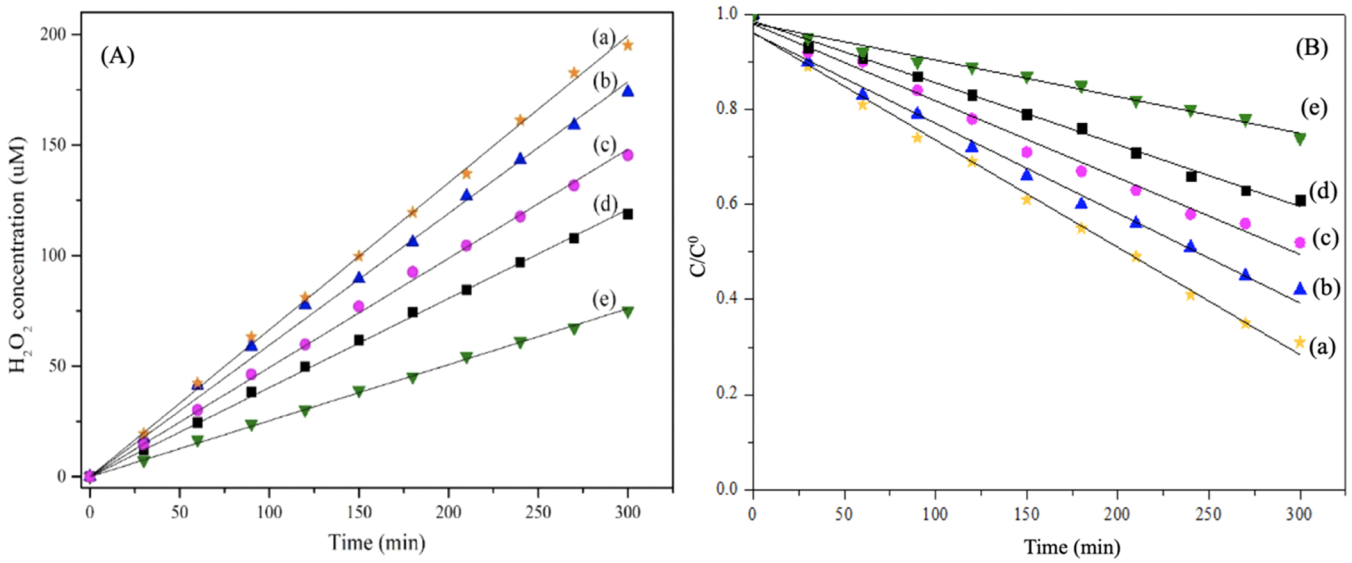

Figure 9. Time-dependent photocatalytic (A) formation and (B) decomposition of H_2O_2 effected by the (a) RFM-H, (b) RFM, (c) RF, (d) RFm-180, and (e) RFm resins.

shifts for the RFM and RFm resins could be attributed to the formation of a mid-gap during the copolymerization process associated with the sp^2/sp^3 rehybridization of carbon atoms in the resorcinol and nitrogen-enriched units.[38,39] In Figure 7C, the PL spectra of the resin photocatalysts were obtained under an excitation wavelength of 325 nm. The emission wavelengths of the resin-based photocatalysts are in the range of 400−700 nm. The PL intensities of the RFm and RFM decrease by incorporating melem units (melem and melamine), suggesting that the formation of tri-s-triazine (heptazine) structures by thermal condensation of melamine may reduce the recombination rate of photogenerated electrons and holes.

Figure 8A shows the electrochemical impedance spectra (EIS) of the resins that have relatively low charge resistances, which are supportive of photocatalytic reactions. The flat band potential of the resins was measured at a fixed frequency of 500 Hz on the electrochemical three-electrode system. The resins are typical n-type semiconductors observed from the slope of the Mott−Schottky plot. The flat band potential determined by the *X*-intercept in the linear region of the Mott−Schottky plot was converted to common potential representation related to the normal hydrogen electrode (NHE). In Figure 8C, the band-gap energy levels of the resins are established by the combination of the band-gap energy and the flat band potential that are obtained from the Tauc and Mott−Schottky plots, respectively. The reaction potentials for two-electron reduction of oxygen (0.68 V) and oxidation of water (1.23 V) are located within the band-gap energy level of the resins, suggesting that the resin photocatalysts are feasible for facilitating the photocatalytic H_2O-to-H_2O_2 reactions.

Photocatalytic H_2O-to-H_2O_2 Reaction. A calibration curve for H_2O_2 concentrations related to the corresponding absorbance at 454 nm using the copper-DMP method for the determination of H_2O_2 concentration from photocatalytic generation and decomposition was developed. Figure 9A shows the time-dependent photocatalytic H_2O-to-H_2O_2 reaction by the resins. The RFM is more effective than the RF and RFm under the visible-light irradiation. In the presence of the RFM resin (40 mg), accumulated 174 μM of H_2O_2 (see Table 1) under the 5 h visible-light irradiation (i.e., 870 μM of

Table 1. Rate Constants for Photocatalytic H_2O_2 Formation (k_f) and Decomposition (k_d) by the Resin Photocatalysts

resins	accumulated H_2O_2 (μmol)	k_f (μM min^{-1})	k_d (min^{-1})
RFM-H	195	0.65	0.0023
RFM	174	0.58	0.0019
RF	134	0.44	0.0016
RFm-180	109	0.36	0.0013
RFm	65	0.21	0.0008

https://doi.org/10.1021/acsomega.2c02371
ACS Omega 2022, 7, 23727−23735

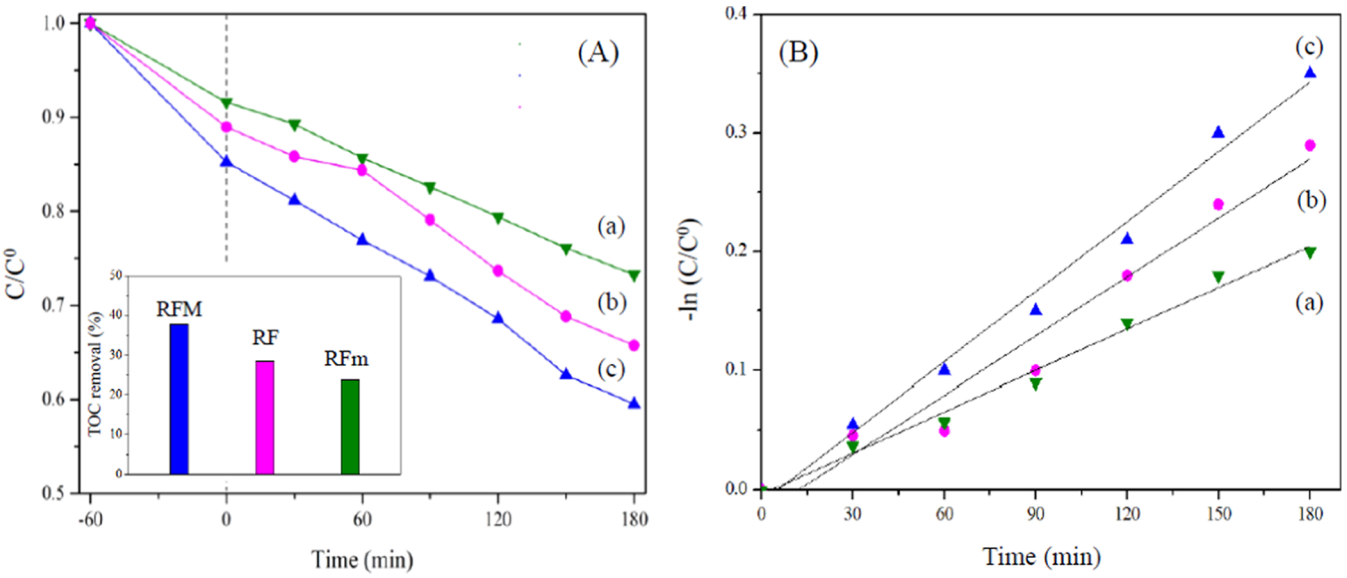

Figure 10. (A) Time-dependent photocatalytic oxidation of methylene blue (3×10^{-5} M) by the RF, RFm, and RFM resins and (B) pseudo-first order rate constant plots for the resins. (Inset in (A): TOC removal efficiencies for photocatalytic oxidation of methylene blue under the 3 h visible-light irradiation).

H_2O_2/g/h) could be obtained. Melem, being the main active matter, could be transformed to 1,4-endoperoxide species during photocatalysis which further induced the formation of H_2O_2.[36] Additionally, one-electron transfer of the O_2 reaction ($O_2 \rightarrow H_2O$) could be effectively suppressed by heptazine during light irradiation.[40]

With an increase of the acidic concentration to 8 M (H_2SO_4) during the copolymerization process, the photocatalytic H_2O_2 yield could further be improved, i.e., 975 μM H_2O_2/g/h (accumulated 195 μM of H_2O_2) (Table 1) for the 5 h visible-light irradiation by the RFM-H resin (see Figure 9). The better photocatalytic H_2O_2 yield by the RFM-H resin may be related to the sulfur-mediated copolymerization which potentially influences texture, electronic and optical properties of the resin. The triazine units seem to be an inactive matter in the RFm resin. Compared to the heptazine structure, triazine has a less ability to induce formation of 1, 4-endoperoxide species.

After the hydrothermal treatment of the RFm resin at 453 K for 24 h, the generated RFm-180 resin with more conducting structure could increase the photocatalytic H_2O_2 yield by 68% if compared with the RFm (accumulated 65 μmol H_2O_2) (Table 1). Yet, the photocatalytic H_2O_2 yield by the RFm-180 resin was less than that by the RF one, suggesting that the triazine unit could distort the inherent phenolic resin structure, which caused a rapid recombination of photogenerated electrons and holes.

The photocatalytic H_2O-to-H_2O_2 reaction may also involve the decomposition of H_2O_2. The reaction kinetics for photocatalytic H_2O_2 formation (k_f) and decomposition (k_d) were thus studied. Generally, the H_2O_2 formation and decomposition rates could be governed by the pseudo-zero-order and pseudo-first-order reaction kinetics, respectively. By the Equation ($[H_2O_2] = (k_f/k_d)(1 - \exp(-k_d t))$), the reaction rate constants for the resin photocatalysts could be obtained (see Table 1). As shown in Figure 9A, the RFM resin with the incorporation of melem accounts for more photocatalytic H_2O_2 yields under the visible-light irradiation than the RF and RFm ones. For the photocatalytic H_2O-to-H_2O_2 reaction, the relatively high H_2O_2 formation k_f accompanies with a high H_2O_2 decomposition k_d, having the H_2O_2 formation equilibrium constant of 280 μM approximately.

Methylene blue, being a representative dye in industry, was used as an organic model pollutant for studying photocatalytic oxidation effected by the resins under the visible light irradiation (λ > 400 nm) at 298 K. The time-dependent photocatalytic oxidation of methylene blue (3×10^{-5} M) effected by the RF, RFm, and RFM resins is shown in Figure 10. The RFM resin photocatalyst that accumulated 174 μM of H_2O_2 (see Table 1) under the 5 h visible-light irradiation has a relatively high reaction rate (pseudo-first-order) for photocatalytic oxidation of methylene blue. Correspondingly, the removal efficiency of TOC for photocatalytic oxidation of methylene blue under the 3 h visible-light irradiation by the RFM resin is 38% that is greater than those by the RF and RFm resins. A similar performance for the photocatalytic H_2O-to-H_2O_2 reaction by the resin photocatalysts was also observed. The photocatalytic H_2O_2 may play a critical role in oxidation of methylene blue.

Reactive oxygen species (ROS) being oxygen-containing radicals are capable of independent existence with one or more unpaired electrons. Reactive oxygen species are often expanded to include reactive oxygen-containing compounds without unpaired electrons, such as H_2O_2. Photocatalytic oxidation of methylene blue could involve direct oxidation by photogenerated holes (h^+) and ROS (H_2O_2, hydroxyl free radicals ($^\bullet OH$) and superoxide free radicals ($^\bullet O_2^-$)). The reduction potentials of the strong ROS such as $H_2O/^\bullet OH$ (2.7 V vs NHE) and $O_2/^\bullet O_2^-$ (0.1 V vs NHE) are not within the band-gap energy level of the resins between 0.28 and 2.39 V (see Figure 8), suggesting that the formation of free radical ROS from H_2O and O_2 may be unfavorable during light irradiation. However, the photocatalytic H_2O-to-H_2O_2 reaction for $H_2O_2/^\bullet OH$ (0.38 V vs NHE) and photogenerated h^+ could account for the oxidation of methylene blue.

Other factors (such as pH) on the H_2O-to-H_2O_2 converting efficiency and methylene blue oxidation performance were thus considered. The effect of pH (1−9 adjusted by HCl (1 M) and

https://doi.org/10.1021/acsomega.2c02371
ACS Omega 2022, 7, 23727−23735

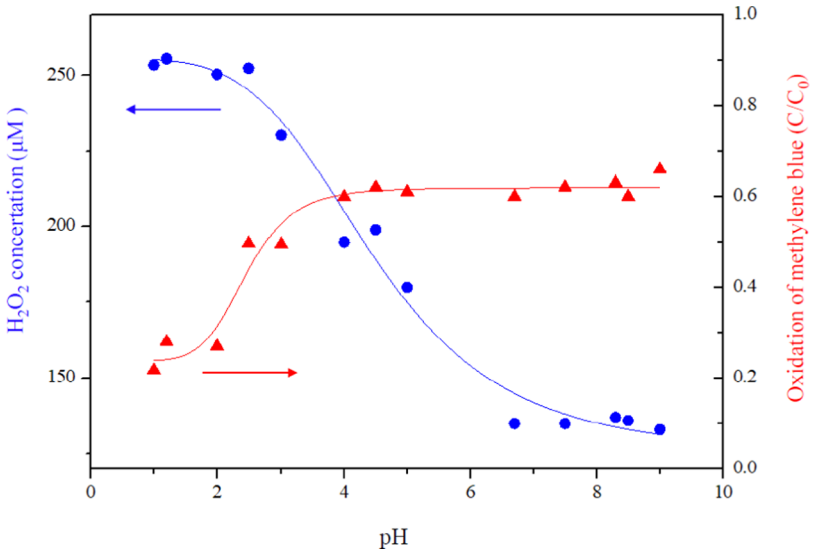

Figure 11. Effect of pH on the photocatalytic H_2O-to-H_2O_2 reaction and oxidation of methylene blue (3×10^{-5} M) by the RFM resin under the visible-light irradiation for 5 h.

NaOH (1 M)) on the photocatalytic H_2O-to-H_2O_2 reaction and oxidation of methylene blue by the RFM resin is shown in Figure 11. At pH 1.0−2.6, the accumulated H_2O_2 is about 250 μM within the 5 h irradiation by RFM and decreases to 180 μM of H_2O_2 as the pH increases to 6.8−9.0. Accordingly, H^+ can prompt the photocatalytic H_2O-to-H_2O_2 reaction. In the presence of high concentration H_2O_2 with the induced ROS ($^{\bullet}OH$), methylene blue could be effectively oxidized (40−80% approximately) by the RFM resin at pH 1−4. At pH 4−9, as the photocatalytic H_2O_2 yields decrease, the photogenerated h^+ could alternatively account for the steady conversion (40%) for oxidation of methylene blue.

CONCLUSIONS

A novel nitrogen-enriched resin with the desired band-gap energy (1.83−1.98 eV) for harvesting visible light was prepared using a simple method for the simultaneous photocatalytic H_2O-to-H_2O_2 reaction and oxidation of methylene blue. Under visible light irradiation for 5 h, very high yields of H_2O_2 (870−975 μM H_2O_2/g/h) by the RFM resin photocatalysts could be achieved. The photocatalytic H_2O_2 reaction for ROS ($^{\bullet}OH$) and photogenerated h^+ could account for the high conversion (40% within a 3 h visible-light irradiation) in oxidation of methylene blue. Such unique low-cost metal-free resins demonstrate the visible-light photocatalytic H_2O-to-H_2O_2 reaction, which can synergize with oxidation of organic pollutants in wastewater.

AUTHOR INFORMATION

Corresponding Author

H. Paul Wang − *Department of Environmental Engineering, National Cheng Kung University, Tainan 70101, Taiwan;* orcid.org/0000-0001-7272-8031; Email: wanghp@ncku.edu.tw

Authors

Je-Wei Hsu − *Department of Environmental Engineering, National Cheng Kung University, Tainan 70101, Taiwan*

Ling-Wei Wei − *Department of Environmental Engineering, National Cheng Kung University, Tainan 70101, Taiwan*

Wan-Ru Chen − *Department of Environmental Engineering, National Cheng Kung University, Tainan 70101, Taiwan*

Shou-Heng Liu − *Department of Environmental Engineering, National Cheng Kung University, Tainan 70101, Taiwan*

Complete contact information is available at: https://pubs.acs.org/10.1021/acsomega.2c02371

Author Contributions

J.W.H. designed the concept and drafted the manuscript. L.W.W. provided the support of the literature search and manuscript revision. W.R.C., S.H.L., and H.P.W. supervised the research work and revised the manuscript. All authors have read and agreed to the published version of the manuscript.

Notes

The authors declare no competing financial interest.

ACKNOWLEDGMENTS

The financial supports of the Taiwan Ministry of Science and Technology (MOST 110-2221-E-006-107-MY2, 109-2221-E-006-042-MY3, and 108-2221-E-006-165-MY3) are gratefully acknowledged.

REFERENCES

(1) Sharma, A.; Ahmad, J.; Flora, S. J. S. Application of advanced oxidation processes and toxicity assessment of transformation products. *Environ. Res.* **2018**, *167*, 223−233.

(2) Miklos, D. B.; Remy, C.; Jekel, M.; Linden, K. G.; Drewes, J. E.; Hübner, U. Evaluation of advanced oxidation processes for water and wastewater treatment−A critical review. *Water Res.* **2018**, *139*, 118−131.

(3) Jung, E.; Shin, H.; Hooch Antink, W.; Sung, Y. E.; Hyeon, T. Recent advances in electrochemical oxygen reduction to H_2O_2: catalyst and cell design. *ACS Energy Lett.* **2020**, *5*, 1881−1892.

(4) Tsukamoto, D.; Shiro, A.; Shiraishi, Y.; Sugano, Y.; Ichikawa, S.; Tanaka, S.; Hirai, T. Photocatalytic H_2O_2 production from ethanol/O_2 system using TiO_2 loaded with Au-Ag bimetallic alloy nanoparticles. *ACS Catal.* **2012**, *2*, 599−603.

(5) Gemo, N.; Menegazzo, F.; Biasi, P.; Sarkar, A.; Samikannu, A.; Raut, D. G.; Mikkola, J. P.; et al. TiO_2 nanoparticles vs. TiO_2 nanowires as support in hydrogen peroxide direct synthesis: the influence of N and Au doping. *RSC Adv.* **2016**, *6*, 103311−103319.

(6) Hirakawa, H.; Shiota, S.; Shiraishi, Y.; Sakamoto, H.; Ichikawa, S.; Hirai, T. Au nanoparticles supported on $BiVO_4$: effective inorganic photocatalysts for H_2O_2 production from water and O_2 under visible light. *ACS Catal.* **2016**, *6*, 4976−4982.
(7) Kumar, S.; Baruah, A.; Tonda, S.; Kumar, B.; Shanker, V.; Sreedhar, B. Cost-effective and eco-friendly synthesis of novel and stable N-doped ZnO/gC_3N_4 core-shell nanoplates with excellent visible-light responsive photocatalysis. *Nanoscale* **2014**, *6*, 4830−4842.
(8) Shiraishi, Y.; Kanazawa, S.; Tsukamoto, D.; Shiro, A.; Sugano, Y.; Hirai, T. Selective hydrogen peroxide formation by titanium dioxide photocatalysis with benzylic alcohols and molecular oxygen in water. *ACS Catal.* **2013**, *3*, 2222−2227.
(9) Shiraishi, Y.; Sugano, Y.; Ichikawa, S.; Hirai, T. Visible light-induced partial oxidation of cyclohexane on WO_3 loaded with Pt nanoparticles. *Catal. Sci. Technol.* **2012**, *2*, 400−405.
(10) Teranishi, M.; Naya, S. I.; Tada, H. Temperature-and pH-dependence of hydrogen peroxide formation from molecular oxygen by gold nanoparticle-loaded titanium (IV) oxide photocatalyst. *J. Phys. Chem. C* **2016**, *120*, 1083−1088.
(11) Baran, T.; Wojtyła, S.; Minguzzi, A.; Rondinini, S.; Vertova, A. Achieving efficient H_2O_2 production by a visible-light absorbing, highly stable photosensitized TiO_2. *Appl. Catal., B* **2019**, *244*, 303−312.
(12) Jeon, D.; Kim, N.; Bae, S.; Han, Y.; Ryu, J. WO_3/conducting polymer heterojunction photoanodes for efficient and stable photo-electrochemical water splitting. *ACS Appl. Mater. Interfaces* **2018**, *10*, 8036−8044.
(13) Liu, Y.; Yang, S.; Zhang, S.; Wang, H.; Yu, H.; Cao, Y.; Peng, F. Design of cocatalyst loading position for photocatalytic water splitting into hydrogen in electrolyte solutions. *Int. J. Hydrogen Energy* **2018**, *43*, 5551−5560.
(14) Teranishi, M.; Naya, S. I.; Tada, H. In situ liquid phase synthesis of hydrogen peroxide from molecular oxygen using gold nanoparticle-loaded titanium(IV) dioxide photocatalyst. *J. Am. Chem. Soc.* **2010**, *132*, 7850−7851.
(15) Zheng, H. B.; Chen, W.; Gao, H.; Wang, Y. Y.; Guo, H. Y.; Guo, S. Q.; Tang, Z. L.; Zhang, J. Y. Melem: an efficient metal-free luminescent material. *J. Mater. Chem. C* **2017**, *5*, 10746−10753.
(16) Niu, P.; Yin, L. C.; Yang, Y. Q.; Liu, G.; Cheng, H. M. Increasing the visible light absorption of graphitic carbon nitride (Melon) photocatalysts by homogeneous self-modification with nitrogen vacancies. *Adv. Mater.* **2014**, *26*, 8046−8052.
(17) Attallah, M. F.; Borai, E. H.; Shady, S. A. Kinetic investigation for sorption of europium and samarium from aqueous solution using resorcinol-formaldehyde polymeric resin. *J. Radioanal. Nucl. Chem.* **2014**, *299*, 1927−1933.
(18) ElKhatat, A. M.; Al-Muhtaseb, S. A. Advances in tailoring resorcinol-formaldehyde organic and carbon gels. *Adv. Mater.* **2011**, *23*, 2887−2903.
(19) Fang, X.; Liu, S.; Zang, J.; Xu, C.; Zheng, M. S.; Dong, Q. F.; Sun, D.; Zheng, N. Precisely controlled resorcinol−formaldehyde resin coating for fabricating core-shell, hollow, and yolk-shell carbon nanostructures. *Nanoscale* **2013**, *5*, 6908−6916.
(20) Li, J.; Wang, X.; Wang, Y.; Huang, Q.; Dai, C.; Gamboa, S.; Sebastian, P. J. Structure and electrochemical properties of carbon aerogels synthesized at ambient temperatures as supercapacitors. *J. Non-Cryst. Solids* **2008**, *354*, 19−24.
(21) Zhang, G.; Ni, C.; Liu, L.; Zhao, G.; Fina, F.; Irvine, J. T. Macro-mesoporous resorcinol−formaldehyde polymer resins as amorphous metal-free visible light photocatalysts. *J. Mater. Chem. A* **2015**, *3*, 15413−15419.
(22) Shiraishi, Y.; Takii, T.; Hagi, T.; Mori, S.; Kofuji, Y.; Kitagawa, Y.; Hirai, T.; et al. Resorcinol-formaldehyde resins as metal-free semiconductor photocatalysts for solar-to-hydrogen peroxide energy conversion. *Nat. Mater.* **2019**, *18*, 985−993.
(23) Akhundi, A.; Badiei, A.; Ziarani, G. M.; Habibi-Yangjeh, A.; Muñoz-Batista, M. J.; Luque, R. Graphitic carbon nitride-based photocatalysts: toward efficient organic transformation for value-added chemicals production. *Mol. Catal.* **2020**, *488*, No. 110902.
(24) Ma, L.; Fan, H.; Fu, K.; Lei, S.; Hu, Q.; Huang, H.; He, G. Protonation of graphitic carbon nitride ($g\text{-}C_3N_4$) for an electrostatically self-assembling carbon@$g\text{-}C_3N_4$ core-shell nanostructure toward high hydrogen evolution. *ACS Sustainable Chem. Eng.* **2017**, *5*, 7093−7103.
(25) Wang, Y.; Wu, N.; Liu, C.; Albolkany, M. K.; Wang, M.; Wang, Y.; Liu, B.; et al. Stimuli-responsive anisotropic actuation of melem-formaldehyde polymer. *Mater. Horizons* **2020**, *7*, 149−156.
(26) Akhundi, A.; Habibi-Yangjeh, A.; Abitorabi, M.; Rahim Pouran, S. Review on photocatalytic conversion of carbon dioxide to value-added compounds and renewable fuels by graphitic carbon nitride-based photocatalysts. *Catal. Rev.* **2019**, *61*, 595−628.
(27) Che, W.; Su, H.; Zhao, X.; Li, Y.; Zhang, H.; Zhou, W.; Liu, Q.; et al. An on-demand solar hydrogen-evolution system for unassisted high-efficiency pure-water splitting. *J. Mater. Chem. A* **2019**, *7*, 17315−17323.
(28) Habibi-Yangjeh, A.; Asadzadeh-Khaneghah, S.; Feizpoor, S.; Rouhi, A. Review on heterogeneous photocatalytic disinfection of waterborne, airborne, and foodborne viruses: Can we win against pathogenic viruses? *J. Colloid Interface Sci.* **2020**, *580*, 503−514.
(29) Asadzadeh-Khaneghah, S.; Habibi-Yangjeh, A. $g\text{-}C_3N_4$/carbon dot-based nanocomposites serve as efficacious photocatalysts for environmental purification and energy generation: a review. *J. Cleaner Prod.* **2020**, *276*, No. 124319.
(30) Jürgens, B.; Irran, E.; Senker, J.; Kroll, P.; Müller, H.; Schnick, W. Melem (2, 5, 8-triamino-tri-s-triazine), an important intermediate during condensation of melamine rings to graphitic carbon nitride: Synthesis, structure determination by X-ray powder diffractometry, solid-state NMR, and theoretical studies. *J. Am. Chem. Soc.* **2003**, *125*, 10288−10300.
(31) Wang, Y.; Wu, N.; Liu, C.; Albolkany, M. K.; Wang, M.; Wang, Y.; Liu, B.; et al. Stimuli-responsive anisotropic actuation of melem-formaldehyde polymer. *Mater Horizons* **2020**, *7*, 149−156.
(32) Kosaka, K.; Yamada, H.; Matsui, S.; Echigo, S.; Shishida, K. Comparison among the methods for hydrogen peroxide measurements to evaluate advanced oxidation processes: application of a spectrophotometric method using copper (II) ion and 2,9-dimethyl-1, 10-phenanthroline. *Environ. Sci. Technol.* **1998**, *32*, 3821−3824.
(33) Abdelhafeez, I. A.; Yao, Q.; Wang, C.; Su, Y.; Zhou, X.; Zhang, Y. Green synthesis of ultrathin edge-activated foam-like carbon nitride nanosheets for enhanced photocatalytic performance under visible light irradiation. *Sustainable Energy Fuels* **2019**, *3*, 1764−1775.
(34) Lin, L.; Ou, H.; Zhang, Y.; Wang, X. Tri-s-triazine-based crystalline graphitic carbon nitrides for highly efficient hydrogen evolution photocatalysis. *ACS Catal.* **2016**, *6*, 3921−3931.
(35) Paju, J.; Pehk, T.; Christjanson, P. Structure of phenol-formaldehyde polycondensates. *Proc. Estonian Acad. Sci.* **2009**, *58*, 45−52.
(36) Shiraishi, Y.; Kanazawa, S.; Sugano, Y.; Tsukamoto, D.; Sakamoto, H.; Ichikawa, S.; Hirai, T. Highly selective production of hydrogen peroxide on graphitic carbon nitride ($g\text{-}C_3N_4$) photocatalyst activated by visible light. *ACS Catal.* **2014**, *4*, 774−780.
(37) Zhou, H.; Xu, S.; Su, H.; Wang, M.; Qiao, W.; Ling, L.; Long, D. Facile preparation and ultra-microporous structure of melamine-resorcinol-formaldehyde polymeric microspheres. *Chem. Commun.* **2013**, *49*, 3763−3765.
(38) Gomis-Berenguer, A.; Velasco, L. F.; Velo-Gala, I.; Ania, C. O. Photochemistry of nanoporous carbons: Perspectives in energy conversion and environmental remediation. *J. Colloid Interface Sci.* **2017**, *490*, 879−901.
(39) Velasco, L. F.; Lima, J. C.; Ania, C. Visible-light photochemical activity of nanoporous carbons under monochromatic light. *Angew. Chem., Int. Ed.* **2014**, *53*, 4146−4148.
(40) Shiraishi, Y.; Kanazawa, S.; Kofuji, Y.; Sakamoto, H.; Ichikawa, S.; Tanaka, S.; Hirai, T. Sunlight-driven hydrogen peroxide production from water and molecular oxygen by metal-free photocatalysts. *Angew. Chem., Int. Ed.* **2014**, *53*, 13454−13459.

https://doi.org/10.1021/acsomega.2c02371
ACS Omega 2022, 7, 23727−23735